ACS APPLIED MATERIALS & INTERFACES

Letter

www.acsami.org

Nanoparticle-Induced Grain Growth of Carbon-Free Solution-Processed $CuIn(S,Se)_2$ Solar Cell with 6% Efficiency

Yongan Cai,[†,‡] John C. W. Ho,[†,§,‡] Sudip K. Batabyal,[†,*] Wei Liu,[⊥] Yun Sun,[⊥] Subodh G. Mhaisalkar,[†,§] and Lydia H. Wong[†,§,*]

[†]Energy Research Institute @ NTU (ERI@N), Nanyang Technological University, Research Techno Plaza, Singapore 637553

[§]School of Materials Science & Engineering, Nanyang Technological University, Singapore 639798

[⊥]Institute of Photoelectron, College of Information Technical Science, Nankai University, Tianjin 300071, China

Supporting Information

ABSTRACT: Chalcopyrite-based solar cell deposited by solution processes is of great research interest because of the ease of fabrication and cost effectiveness. Despite the initial promising results, most of the reported methods encounter challenges such as limited grain growth, carbon-rich interlayer, high thermal budget, and the presence of secondary Cu-rich phases, which limit the power conversion efficiency (PCE). In this paper, we develop a new technique to deposit large grain, carbon-free CISSe absorber layers from aqueous nanoparticle/precursor mixture which resulted in a solar cell with PCE of 6.2%. $CuCl_2$, $InCl_3$, and thiourea were mixed with CuS and In_2S_3 nanoparticles in water to form the unique nanoparticle/precursor solution. The Carbon layer formation was prevented because organic solvents were not used in the precursor. The copper-rich (CuS) nanoparticles were intentionally introduced as nucleation sites which accelerate grain growth. In the presence of nanoparticles, the grain size of CISSe film increased by a factor of 7 and the power conversion efficiency of the solar cell is 85% higher than the device without nanoparticle. This idea of using nanoparticles as a means to promote grain growth can be further exploited for other types of chalcopyrite thin film deposited by solution methods.

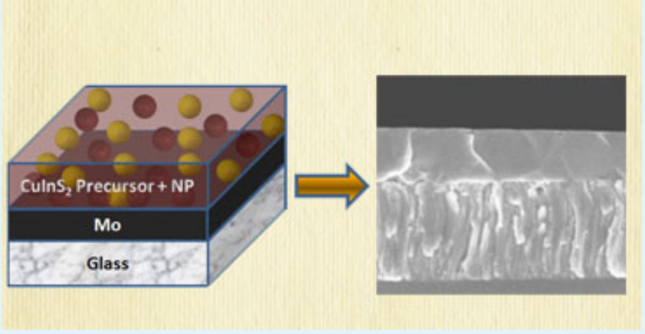

KEYWORDS: *CuIn(S,Se), CIGS, photovoltaics, spray pyrolysis, nanoparticle, grain growth, selenization*

INTRODUCTION

$Cu(In,Ga)Se_2$ (CIGS) is a good light absorber materials and has been reported to yield one of the highest power conversion efficiencies for thin film photovoltaic devices because of its high absorption coefficient and appropriate band gap. Despite the promising efficiency level,[1] the production cost of the conventional vacuum-based processes such as coevaporation or sputtering[2−4] prevents the widespread commercialization of CIGS-based solar cells. In this regard, CIGS deposited by solution processes[5−13] are promising because of relatively simple and low-cost procedures. To date, the reported solution-based approaches for CIGS absorber layer deposition include electrochemical,[6,13] spray or spin-coating of organometallic precursors,[5] screen printing of CIGS or component metal pastes,[7,8] ink jet printing of nanoparticle-based ink,[9,12] and hydrazine-based approach.[14]

Even though the nanoink approach allows possibility of controlling the composition uniformity, most of these approaches do not result in significant grain growth and hence limit the power conversion efficiency.[11,9,15] The formation of carbon-rich interlayer between Mo substrate and CIS thin film was also frequently reported to limit the power conversion efficiency.[16−18] Jeong et al.[12] reported a method with a very small amount of C content but the selenization was carried out at 520 °C for 1 h. The high thermal budget process is not desirable for solar cell fabrication on flexible polymeric substrates. The Hillhouse group recently reported a nanoink-based device with 12% efficiency by using Na doping to induce grain growth; however, a toxic KCN treatment was used to remove unwanted Cu-rich residues.[19] Therefore, it is clear that challenges associated with solution-processed CIGS thin film such as limited grain growth, carbon-rich interlayer, high thermal budget, and the presence of secondary Cu-rich phases still need to be addressed in order to realize a low-cost, high-efficiency CIGS device from solution processes.

In the vacuum-deposited CIGS film, it is well-established that a Cu-rich phase facilitates grain growth[4] even though the final CIGS film should be free of the Cu-rich phase because they can cause electrical shorts. Inspired by this approach, we used Cu-rich nanoparticles to help grain growth together with Cu-poor precursor to yield a final absorber film that is free from Cu-rich phases. The absorber layer solution contains CuS and In_2S_3

Received: December 11, 2012
Accepted: February 19, 2013
Published: February 19, 2013

   dx.doi.org/10.1021/am303057z | ACS Appl. Mater. Interfaces 2013, 5, 1533−1537

nanoparticles mixed with a clear solution of $CuCl_2$, $InCl_3$, and thiourea in water, without any organic solvents. By using excess Sulfur in the precursor, we managed to avoid the molybdenum oxide formation on Mo substrate during spray deposition as well as preventing the formation of C-rich film. $CuIn(S,Se)_2$ (CISSe) thin film with appropriate grain size and composition was achieved after selenization and solar cell device with 6.2% power conversion efficiency was demonstrated. In a nutshell, the key advantages of our novel approach are (1) all synthesis routes were carried out in aqueous solution without any organic solvents to prevent the formation of Carbon-rich layer, (2) grain growth was assisted by the presence of Cu-rich nanoparticles in the precursor solution, and (3) no toxic chemicals (such as hydrazine or KCN etch) were used in the synthesis and device fabrication procedures.

EXPERIMENTAL SECTION

Nanoparticle Synthesis. CuS nanoparticles were synthesized by mixing Na_2S and $CuCl_2$ in the molar ratio of 2:1 in deionized water at room temperature. Similarly, In_2S_3 nanoparticles were synthesized by mixing Na_2S and $InCl_3$ in the ratio of 5:2 in deionized water at room temperature. The resultant mixture was centrifuged and washed with deionized water before drying in vacuum. The as synthesized nanopartciles were characterized by FESEM and XRD (the results are shown in ESI). The FESEM analysis shows that the sizes of both the nanoparticles are in the range of 20 to 50 nm. From the XRD analysis, we found the Indium sulfide nanoparticles are amorphous in nature but the crystallographic phase of copper sulfide nanoparticles is identical with the digenite phase of Cu_9S_5 with the JCPDS number 00−047−1748.

Precursor Film Preparation. The Cu-poor precursor was made by mixing 8 mL of 0.01 M $CuCl_2$, 10 mLof 0.01 M $InCl_3$, and 0.5 mL of 1.0 M thiourea in water. This Cu-poor precursor was then sprayed on top of preheated Mo-coated glass at 120 °C (Figure 1a) to form a thin CIS film. Subsequently, the temperature of the hot plate was increased slowly during spray to reach the final temperature of 350 °C. The spray rate was kept at approximately 1−2 mL/min. Another precursor was designed by mixing nanoparticle with the aqueous precursor (np-precursor). In a typical procedure, this np-precursor solution was synthesized by adding 0.2 mmol of CuS and 0.3 mmol of In_2S_3 nanoparticles aqueous dispersion with the solution containing 65 mL of 0.01 M $CuCl_2$, 40 mL of 0.01 M $InCl_3$, and 5 mL of 1.0 M thiourea ($SC(NH_2)_2$). The precursor solution was sprayed onto Mo-coated glass heated to a temperature of 320−350 °C to form a continuous film. Thereafter, a second precursor solution was prepared by mixing 8 mL of 0.01 M $CuCl_2$, 10 mL of 0.01 M $InCl_3$, and 0.5 mL of 1.0 M thiourea in water to form a Cu-poor precursor solution. It was then sprayed on top of the film formed previously (Figure 1b). The final Cu/In ratio were obtained as about 0.85 as confirmed by EDX analysis. To prevent the formation of a carbon interlayer after selenization, we judicially chose water as the solvent in all synthesis steps.

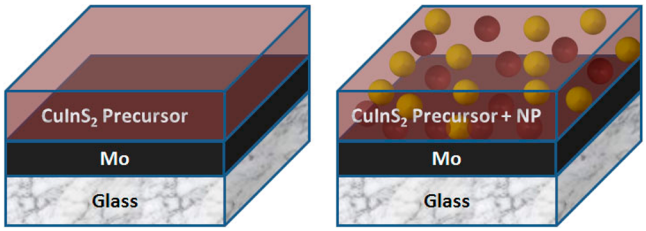

Figure 1. Schematic diagram to illustrate the two precursor film design: (a) Precursor solution approach and (b) Mixed nanoparticles/precursor solution approach containing CuS nanoparticle and In_2S_3 nanoparticles.

Device Fabrication. The sprayed CIS films were annealed in Se vapor, selenization, at temperature of 480−500 °C to form CISSe film. Selenization allows the tuning of bandgap by the substitution of S with Se and induced grain growth in the absorber layer. Thereafter, CdS buffer layer (∼50 nm) was deposited by chemical bath deposition. Then, i-ZnO and Al:ZnO (TCO layer) were sputtered on top of CdS followed by thermal evaporation of Al electrode on top of the TCO layer. CdS deposition was carried out in the bath containing aqueous solution of cadmium acetate, ammonium acetate and thiourea at 85 °C. The pH of the bath was adjusted to 9.0 by ammonium hydroxide. The TCO layer used was aluminum doped zinc oxide and deposited via DC sputtering with an applied power of 200 W. After thermal evaporation of Al electrode, the cells were isolated by mechanical scribing with a cell area of 0.08 cm^2.

Characterization. Cross-section images of samples were obtained by Field Emission Scanning Electron Microscope (FESEM), JEOL JSM-7600F, with an energy-dispersive X-ray (EDX) spectrometer attachment. The crystal structures of the samples were studied using X-ray Diffraction (XRD) by Bruker D8 Advance Diffractometer. The current density−voltage (J−V) characteristics of the $CuIn(S,Se)_2$ devices were measured in ambient conditions under AM 1.5G illumination (100 mW/cm^2) using a Keithley SMU 2400 sourcemeter. The light intensity was calibrated by using an NREL calibrated silicon photodiode.

RESULTS AND DISCUSSIONS

During spray deposition, the proposed chemical reaction of $CuInS_2$ film formation that occurs when the micrometer size precursor droplet landed on the heated substrate is described below

$$CuCl_2{\cdot}nH_2O + InCl_3{\cdot}mH_2O + SC(NH_2)_2 \rightarrow CuInS_2 + Cl_2 + H_2O \ (n \text{ and } m \approx 2)$$

The $CuInS_2$ film is then transformed to $CuIn(S,Se)_2$ after selenization. To confirm the above reaction, we carried out X-ray diffraction experiments. The XRD patterns of the np-precursor and precursor-only films before and after selenization are shown in panels a and b in Figure 2, respectively. Before selenization, the diffraction peaks match well with the standard data sheet (JCPDS No- 85−1575) of $CuInS_2$ without any trace of metal oxides. We believe that the excess sulfur in the precursor prevents the unnecessary oxide formation from the precursors and also protect Mo substrate from oxidation at high temperature. The diffraction patterns of the film after selenization matches that of CISSe (JCPDS no. 36−1311) (Figure 2b) with slight variation in peak positions due to the different S/Se ratio that affects the lattice parameters. The S/Se +Se ratio for the selenized CISSe films was estimated by Rietveld refinement and found to be approximately 0.29−0.41 (Table 1). The increase in the relative intensity of (112) peaks of both films after selenization (Figure 2b) indicate improved crystallinity of these films. This was expected as the spray deposition temperature of 320−350 °C might not be sufficient to induce complete crystallization. The increase in (112) peak intensity also indicates a preferred grain growth along the (112) plane at the expense of (204)/(220) oriented grains, which was observed by NREL group.[20]

The grain growth and morphology of the thin film were studied in details by FESEM. Images a and c in Figure 3 represent the cross-sectional images of the as-deposited film from precursor and np-precursor, respectively. These images

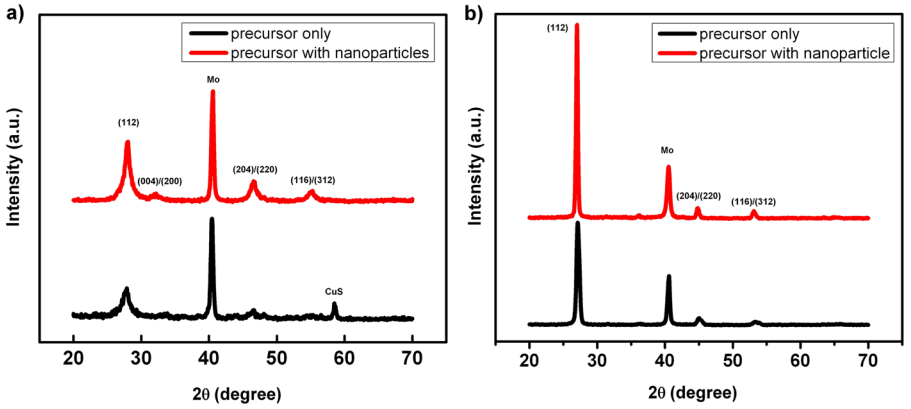

Figure 2. (a) XRD pattern of the as deposited film from the precursor solution and the nanoparticle incorporated precursor solution. (b) XRD pattern of the films after selenization (peaks are indexed according to the JCPDS No- 85−1575).

Table 1. Rietveld Refinement Results of $CuInS_2$ Films before and after Selenization

	lattice parameter		atomic %	
sample	*a* (Å)	*c* (Å)	S (%)	Se (%)
precursor only	5.518	11.254	100	0
precursor with nanoparticle	5.495	11.103	100	0
precursor with nanoparticle −after selenization	5.695	11.501	29	71
precursor only − after selenization	5.664	11.448	41	59

clearly show the formation of a single-layer CISSe thin film. The difference in grain size is not significant from the FESEM cross-sectional images but the roughness on the top surface of nanoparticle-precursor (np-precursor) thin film is higher than the precursor-based film, probably due to the size of nanoparticles.

From the cross-section FESEM images of the absorber layer after selenization, considerable grain growth can be observed (Figure 3b, d). The np-precursor film (Figure 3d) resulted in much larger grains of 600−700 nm, whereas the grains of the selenized film deposited from precursor only are in the range of 100 nm (Figure 3b). The reason for a significant difference in grain size observed between the films can be attributed to the presence of Cu-rich nanoparticles which act as nucleation sites for grain growth. The key idea of incorporating nanoparticles into our precursor spray solution is to promote the formation of Cu-rich regions to mimic the 3 stage coevaporation technique used in high vacuum CIGS deposition.[4] We postulate that the grain growth starts from the Cu-rich and the In-rich

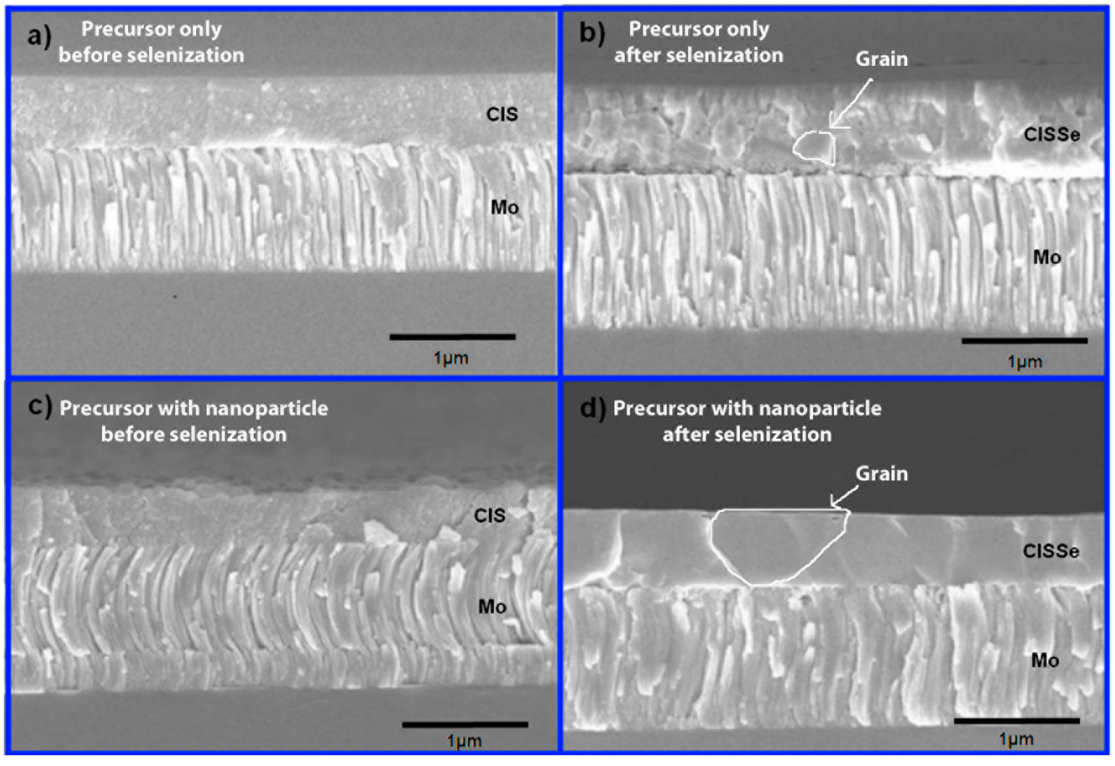

Figure 3. Cross-sectional FESEM image of the as deposited absorber layer from precursor (a) before and (b) after selenization, and from nanoparticle incorporated precursor (c) before and (d) after selenization.

dx.doi.org/10.1021/am303057z | ACS Appl. Mater. Interfaces 2013, 5, 1533−1537

regions, which formed around the CuS nanoparticles and In_2S_3 nanoparticles, respectively. The two regions would subsequently react with each other in the presence of Se at high temperature to form large grain CISSe. The presence of In-rich nanoparticles is important to avoid the formation of CuSe or Cu_2Se phase, which are unfavorable for device performance. Since the formation of CuSe and Cu_2Se phase could be prevented, the toxic KCN etching after selenization, which is commonly used to etch CuSe and Cu_2Se, can be skipped. It should also be noted that the Carbon interlayer between Mo and CISSe, which was reported in many solution processed CIS thin films,[16−18] are not observed in images b and d in Figure 3. EDX analysis further confirmed that the absorber layers were free from Carbon.

To investigate the photovoltaic performance of the absorber layers deposited from these two precursor designs, we fabricated the solar cells by depositing CdS buffer layer, intrinsic ZnO, AZO and metal grid electrode on the absorber layers. We found the np-precursor film (700 nm thick) exhibits higher power conversion efficiency (η = 6.15%) as compared to the device based on precursor film (800 nm thick) (η = 3.47%) (Figure 4). In general, we fabricated 8 devices on the same

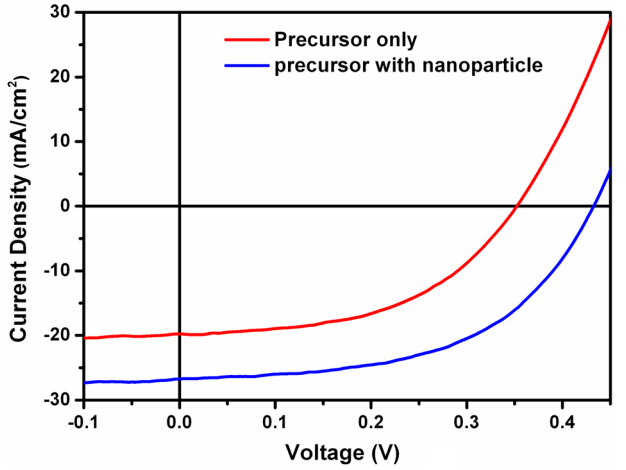

Figure 4. *IV* curve of device fabricated from nanoparticle incorporated precursor (blue) film and precursor film without nanoparticle (red). The active area of both devices was 0.08 cm^2.

substrate and we observed the PCE variation of the np-precursor film was in the range of 5−6%, whereas the variation of the precursor film was in the range of 2.5% to 3.5%. The np-precursor film shows a higher efficiency due to increase in V_{oc} (23%) and J_{sc} (35%) as compared to the precursor film. The enhanced J_{sc} of the np-precursor film can be attributed to the larger grain size with less grain boundary and recombination site, while the higher V_{oc} could be attributed to larger and more uniform interface between CdS and the CISSe layer. The relatively low FF (0.53 and 0.50) is attributed to the inefficient charge collection as a result of non-optimized transparent conducting layer (ZnO/AZO) and top electrode. Our best power conversion efficiency here is comparable to the other nanoparticle-based approaches,[9−11] which does not use any doping to induce grain growth. It should be noted that the highest device efficiency of solution-processed CIGS is 15% and is achieved using toxic hydrazine as a reducing agent.[14]

The effect of absorber layer thickness on device performance is shown in Figure 5. The details on device properties (V_{oc}, J_{sc},

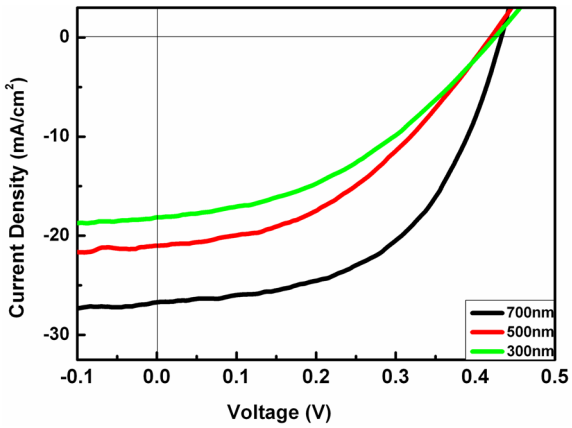

Figure 5. Photovoltaic performance of a nanoparticle-based device with different thicknesses of the absorber layers.

FF) are summarized in table 2. We found that J_{sc} increased from 18.1 mA/cm^2 to 26.7 mA/cm^2 for np- precursor film when the

Table 2. Photovoltaic Performance of a Nanoparticle-Based Device with Different Thicknesses of the Absorber Layers

type	thickness (nm)	V_{oc} (V)	J_{sc} (mA/cm^2)	FF (%)	η (%)
precursor with nanoparticle	300	0.42	18.1	41	3.16
	500	0.42	21.0	43	3.74
	700	0.43	26.7	53	6.15
precursor only	800	0.35	19.8	50	3.47

absorber layer thickness is increased from 300 nm to 700 nm. As absorber layer thickens, more light could be absorbed and hence a higher photogenerated carrier density will be generated and collected at the respective contacts (holes are collected by Mo substrate while electrons are collected by Al electrode). The consistent V_{oc} shows a well-controlled CdS deposition process in all films.

CONCLUSIONS

A new deposition technique to deposit carbon-free CISSe absorber layers from aqueous nanoparticle/precursor mixture without the use of any toxic chemicals has been developed. It was found that the nanoparticle-incorporated precursor promotes grain growth of CISSe absorber layers as the Cu-rich nanoparticles act as nucleation centers for grain growth. In the presence of nanoparticles, the grain size of CISSe film increased by a factor of 7 and the power conversion efficiency of the solar cell device is 6.2%, 85% higher than the device without nanoparticle. This idea of using nanoparticles as a mean to promote grain growth can be further exploited for other types of chalcopyrite thin film deposited by solution processes.

ASSOCIATED CONTENT

Supporting Information

FESEM and XRD data of the individual nanoparticles. This material is available free of charge via the Internet at http://pubs.acs.org.

dx.doi.org/10.1021/am303057z | ACS Appl. Mater. Interfaces 2013, 5, 1533−1537

AUTHOR INFORMATION

Corresponding Author

*E-mail: LydiaWong@ntu.edu.sg (L.H.W.), batabyal@gmail.com (S.K.B.).

Author Contributions

‡Y.C. and J.C.W.H. have contributed equally to this work.

Notes

The authors declare no competing financial interest.

ACKNOWLEDGMENTS

J.H. thanks Economic Development Board (EDB) of Singapore for the scholarship. The authors acknowledge financial supports from A*STAR SERC Printed Photovoltaic Program Grant 1021700143) and the Singapore National Research Foundation CREATE program: "Nanomaterials for Energy and Water Management."

REFERENCES

(1) Jackson, P.; Hariskos, D.; Lotter, E.; Paetel, S.; Wuerz, R.; Menner, R.; Wischmann, W.; Powalla, M. *Prog. Photovoltaics Res. Appl.* **2011**, *19*, 894.

(2) Chirilă, A.; Buecheler, S.; Pianezzi, F.; Bloesch, P.; Gretener, C.; Uhl, A. R.; Fella, C.; Kranz, L.; Perrenoud, J.; Seyrling, S.; Verma, R.; Nishiwaki, S.; Romanyuk, Y. E.; Bilger, G.; Tiwari, A. N. *Nat. Mater.* **2011**, *10*, 857.

(3) Kemell, M.; Ritala, M.; Leskelä, M. *Crit. Rev. Solid State Mater. Sci.* **2005**, *30*, 1.

(4) Repins, I.; Contreras, M. A.; Egaas, B.; DeHart, C.; Scharf, J.; Perkins, C. L.; To, B.; Noufi, R. *Prog. Photovoltaics Res. Appl.* **2008**, *16*, 235.

(5) Hollingsworth, J. A.; Banger, K. K.; Jin, M. H. C.; Harris, J. D.; Cowen, J. E.; Bohannan, E. W.; Switzer, J. A.; Buhro, W. E.; Hepp, A. F. *Thin Solid Films* **2003**, *431−432*, 63.

(6) Calixto, M. E.; Dobson, K. D.; McCandless, B. E.; Birkmire, R. W. *J. The Electrochem. Soc.* **2006**, *153*, G521.

(7) Kaelin, M.; Rudmann, D.; Tiwari, A. N. *Solar Energy* **2004**, *77*, 749.

(8) Vervaet, A.; Burgelman, M.; Clemminck, I.; Casteleyn, M. In *10th European Photovoltaic Solar Energy Conference*; Lisbon, Portugal , 1991; p 900.

(9) Panthani, M. G.; V., A.; Goodfellow, B.; Schmidtke, J. P.; Dunn, L.; Dodabalapur, A.; Barbara, P. F.; Korgel, B. A. *J. Am. Chem. Soc.* **2008**, *130*, 16770.

(10) Guo, Q.; Ford, G. M.; Hillhouse, H. W.; Agrawal, R. *Nano Lett.* **2009**, *9*, 3060.

(11) Akhavan, V. A.; Goodfellow, B. W.; Panthani, M. G.; Reid, D. K.; Hellebusch, D. J.; Adachi, T.; Korgel, B. A. *Energy Environ. Sci.* **2010**, *3*, 1600.

(12) Jeong, S.; Lee, B.-S.; Ahn, S.; Yoon, K.; Seo, Y.-H.; Choi, Y.; Ryu, B.-H. *Energy Environ. Sci.* **2012**, *5*, 7539.

(13) Bhattacharya, R. N.; Oh, M.-K.; Kim, Y. *Sol. Energy Mater. Sol. Cells* **2012**, *98*, 198.

(14) Mitzi, D. B.; Yuan, M.; Liu, W.; Kellock, A. J.; Chey, S. J.; Gignac, L.; Schrott, A. G. *Thin Solid Films* **2009**, *517*, 2158.

(15) Akhavan, V. A.; Goodfellow, B. W.; Panthani, M. G.; Steinhagen, C.; Harvey, T. B.; Stolle, C. J.; Korgel, B. A. *J. Solid State Chem.* **2012**, *189*, 2.

(16) Ahn, S.; Kim, C.; Yun, J. H.; Gwak, J.; Jeong, S.; Ryu, B.-H.; Yoon, K. *J. Phys. Chem. C* **2010**, *114*, 8108.

(17) Kaelin, M.; Rudmann, D.; Kurdesau, F.; Zogg, H.; Meyer, T.; Tiwari, A. N. *Thin Solid Films* **2005**, *480−481*, 486.

(18) Klugius, I.; Miller, R.; Quintilla, A.; Friedlmeier, T. M.; Blázquez-Sánchez, D.; Ahlswede, E.; Powalla, M. *Phys Status Solidi RRL* **2012**, *6*, 297.

(19) Guo, Q.; Ford, G. M.; Agrawal, R.; Hillhouse, H. W. *Prog. Photovolt. Res. Appl.* **2013**, *21*, 64.

(20) Contreras, M. A.; Romero, M. J.; Noufi, R. *Thin Solid Films* **2006**, *511−512*, 51.